OPEN ACCESS

**Scholars International Journal of Chemistry and Material Sciences**
Abbreviated Key Title: Sch Int J Chem Mater Sci
ISSN 2616-8669 (Print) |ISSN 2617-6556 (Online)
Scholars Middle East Publishers, Dubai, United Arab Emirates
Journal homepage: http://saudijournals.com

**Original Research Article**

# Sustainable Utilization of Electric Arc Furnace Slag-derive Nanocomposite Catalyst as Effective Photocatalysts for $CO_2$ Capturing and Reduction under a Continuous Flow Photoreactor into Hydrogen and Methanol

Kingsley Safo[1]*, Felix A. Kwarteng[2], Joseph Boahen[2], Francis Tetteh[3], Emmanuel Afreh[4], Hussien Noby[5], Ahmed H El-Shazly[1]

[1]Department of Chemical and Petrochemicals Engineering, Egypt-Japan University of Science and Technology, New Borg Al-Arab city, Alexandria, Egypt
[2]Materials Science and Engineering Program, School of Innovative Engineering, Egypt-Japan University of Science and Technology (E-JUST), 179 New Borg El-Arab City, Alexandria, Egypt
[3]Department of Agricultural Engineering, Kwame Nkrumah University of Science and Technology (KNUST) PMB KNUST, Kumasi, Ashanti Region, 00233, Ghana
[4]Department of Chemical and Biomolecular Engineering, University of Notre Dame, South Bend, IN 46556, USA
[5]Department of Mechanical Engineering, Faculty of Energy Engineering, Aswan University, Aswan 81528, Egypt

**DOI:** https://doi.org/10.36348/sijcms.2026.v09i02.001 | **Received:** 13.01.2026 | **Accepted:** 07.03.2026 | **Published:** 11.03.2026

***Corresponding author:** Kingsley Safo
Department of Chemical and Petrochemicals Engineering, Egypt-Japan University of Science and Technology, New Borg Al-Arab city, Alexandria, Egypt

## Abstract

This study presents a one-step solvothermal approach for the preparation of Electric Arc Furnace steel slag nanocomposite (EAF-SSNC) aimed at converting $CO_2$ into hydrogen and methanol. The EAF-SSNC was characterized using scanning electron microscopy (SEM), transmission electron microscopy (TEM), and energy-dispersive X-ray spectroscopy (EDX). The SEM analysis revealed a spherical and heterogeneous structure with macropores, while EDX results indicated a composition of 26.3 wt% O, 32.4 wt% Fe, 11.94 wt% Si, 0.27 wt% Ti, 3.26 wt% Al, 2.93 wt% Mg, 20.43 wt% Ca, and 2.47 wt% Mn. X-ray diffraction (XRD) analysis confirmed the presence of multiple crystalline phases, including Andradite, Hematite, and Calcite. The photocatalytic performance of the EAF-SSNC was evaluated under varying dosages (10-60 mg/L) at a reactor temperature of 30°C and a flow rate of 500 µl/min, with a total water volume of 60 ml. The total organic carbon (TOC) levels were quantitatively assessed using a TOC analyzer, and gas chromatography-mass spectrometry (GC-MS) was employed to analyze the liquid products, which revealed that methanol ($CH_3OH$) was the predominant product, whereas HCHO was the minor one. The findings suggest that EAF-SSNC can serve as an effective catalyst for $CO_2$ reduction, addressing environmental concerns associated with steel slag disposal while contributing to sustainable carbon management strategies. This research highlights the potential of utilizing industrial by-products in innovative ways to mitigate environmental impact and promote resource recovery.

**Keywords:** steel Slag; Nanocomposite; Photocatalysis; $CO_2$ reduction; Total Organic Carbon; Methanol.

## 1.0 INTRODUCTION

Anthropogenic carbon dioxide ($CO_2$) emissions remain the primary driver of global warming, and their continued rise threatens to push global mean surface temperature beyond the 1.5 °C threshold identified as critical issue to human health (Dananjayan *et al.*, 2022)(Moon and Cheol, 2018). In parallel with aggressive deployment of renewable energy and efficiency measures, carbon capture, utilization, and storage (CCUS) have emerged as an essential technological pillar to achieve deep decarbonization in carbon intensive sectors such as steelmaking, power generation, and heavy industry(Chen *et al.*, 2022)(Saratu *et al.*, 2021). Among various CCUS strategies, photocatalytic $CO_2$ reduction using semiconductor-based catalysts has attracted particular attention because

**Citation:** Kingsley Safo, Felix A. Kwarteng, Joseph Boahen, Francis Tetteh, Emmanuel Afreh, Hussien Noby, Ahmed H El-Shazly (2026). Sustainable Utilization of Electric Arc Furnace Slag-derive Nanocomposite Catalyst as Effective Photocatalysts for $CO_2$ Capturing and Reduction under a Continuous Flow Photoreactor into Hydrogen and Methanol. *Sch Int J Chem Mater Sci, 9*(2): 66-76.

it enables direct conversion of $CO_2$ and water into value added solar fuels and chemicals, thereby coupling atmospheric carbon management with green energy production(Li *et al*., 2024)(Narindri *et al*., 2024). However, the widespread implementation of photocatalytic $CO_2$ reduction is still constrained by several challenges, including limited light harvesting efficiency, rapid charge recombination, low selectivity toward desired products, and the high cost and environmental burden of conventional catalyst materials(Zhang *et al*., 2023)(Zhao *et al*., 2025)(Fusco *et al*., 2022).

Concurrently, the steel industry generates enormous quantities of solid by products in the form of blast furnace, basic oxygen furnace, and electric arc furnace (EAF) slags, with global production estimated at hundreds of millions of tonnes per year (Tossavainen *et al*., 2007) (Manchisi *et al*., 2020)(Safo *et al*., 2022b)(Dananjayan *et al*., 2022). These slags possess complex chemical and mineralogical compositions, typically rich in CaO, $SiO_2$, $Fe_2O_3$, MgO, and $Al_2O_3$, and have been widely explored as secondary resources in cement manufacture, road construction, and environmental remediation(Fusco *et al*., 2022)(Safo *et al*., 2025)(Zhang *et al*., 2023). Despite these efforts, a substantial fraction of steel slag still accumulates in stockpiles or landfills, leading to land occupation, potential leaching of hazardous components, and underutilization of a strategically important industrial residue(Li *et al*., 2024)(Safo *et al*., 2023b)(Moon and Cheol, 2018). In recent years, steelmaking slag has also been proposed as a promising feedstock for mineral carbonation and $CO_2$ sequestration, where alkaline components react with $CO_2$ to form thermodynamically stable carbonates, thereby providing a permanent and leakage free storage option while simultaneously valorizing an industrial waste(Safo and Badry, 2024) (Zhao *et al*., 2025)(Safo *et al*., 2022a)(Moon and Cheol, 2018)(Chen *et al*., 2022). Studies on direct aqueous and gas solid carbonation of steelmaking slags using flue gas have demonstrated significant $CO_2$ uptake capacities and highlighted operating variables such as temperature, pressure, and liquid to solid ratio as critical parameters governing sequestration performance(Dananjayan *et al*., 2022)(Saratu *et al*., 2021)(Yu and Wang, 2011).

Beyond its role as a reactive alkaline medium for mineral carbonation, steel slag contains iron bearing and silicate phases that can be engineered into functional nanocomposites with catalytic, magnetic, or adsorptive properties(Zhang *et al*., 2023) (Kang *et al*., 2015) (Safo *et al*., 2022b). Transforming slag into photocatalysts offers an attractive pathway to couple $CO_2$ capture and utilization, since the same waste derived material can provide active sites for $CO_2$ activation while addressing the environmental liabilities associated with slag disposal (Zhao *et al*., 2025)*(Safo et al*., 2022a)(Tsakiridis *et al*., 2008)(Das *et al*., 2007). Previous work has shown that carefully designed slag-based nanocomposites exhibit promising activity for the photodegradation of organic dyes under UV and visible light, underscoring their potential as low cost, robust photocatalytic materials (Safo *et al*., 2023a)(Safo *et al*., 2023b). Nevertheless, the application of slag derived nanocomposites in photocatalytic $CO_2$ reduction remains relatively unexplored, and key questions persist regarding optimal synthesis routes, structure property relationships, reaction selectivity, and performance under continuous flow conditions that are relevant to practical process integration *(Zhang et al*., 2023)(Chen *et al*., 2022)(Saratu *et al*., 2021).

To address these gaps, the present study develops a sustainable one step solvothermal approach for preparing an Electric Arc Furnace steel slag nanocomposite (EAF SSNC) and investigates its use as an efficient photocatalyst for $CO_2$ capture and reduction to hydrogen and methanol in a meso scale continuous flow photoreactor. In this route, raw EAF steel slag obtained from an industrial source is subjected to controlled acid treatment, drying, calcination, and milling to yield a nanostructured composite whose composition and morphology are tailored by the intrinsic mineralogy of the slag and the imposed thermal chemical history. Comprehensive physicochemical characterization of the resulting EAF SSNC was performed using scanning electron microscopy (SEM), transmission electron microscopy (TEM), energy dispersive X ray spectroscopy (EDX), Fourier transform infrared spectroscopy (FTIR), and X ray diffraction (XRD) to elucidate its microstructure, elemental distribution, functional groups, and crystalline phases. The photocatalytic performance of EAF SSNC for $CO_2$ reduction was then evaluated under continuous flow operation, using an aqueous medium and controlled catalyst dosages over a range of 10–60 mg $L^{-1}$ at a reactor temperature of 30 °C and a fixed liquid flow rate. Total organic carbon (TOC) measurements and gas chromatography mass spectrometry (GC–MS) analyses were employed to quantify $CO_2$ conversion and identify liquid phase products.

## 2.1 MATERIALS

This study used slag from Ezz steel in Egypt. Nitric acid (69% $HNO_3$), hydrochloric acid (37% HCl), and from the UK (Fisher Scientific Company).

## 2.2 METHODS

### 2.2.1 Synthesis of the photocatalyst

The collected EAF steel slag was washed, dried, and ball milled for 30 minutes before being added to 10 ml of $HNO_3$ in a glass beaker and constantly swirled on a magnetic stirrer at 500 rpm at room temperature for five hours to guarantee total slag dissolution. A dark-green solution was formed when the slag was completely dissolved in the acid. The solution was transferred to a glass dish and dried for one day at 70 °C (24 hours). After drying, the solution's colour changed from greenish to dark orange, suggesting a change in the oxidation state of the iron in the steel slag (Safo *et al*., 2025). The dried samples were pulverized and calcined at 1000 °C for 60 minutes. The resultant sample was named EAF Steel Slag Nanocomposite (EAF-SSNC).

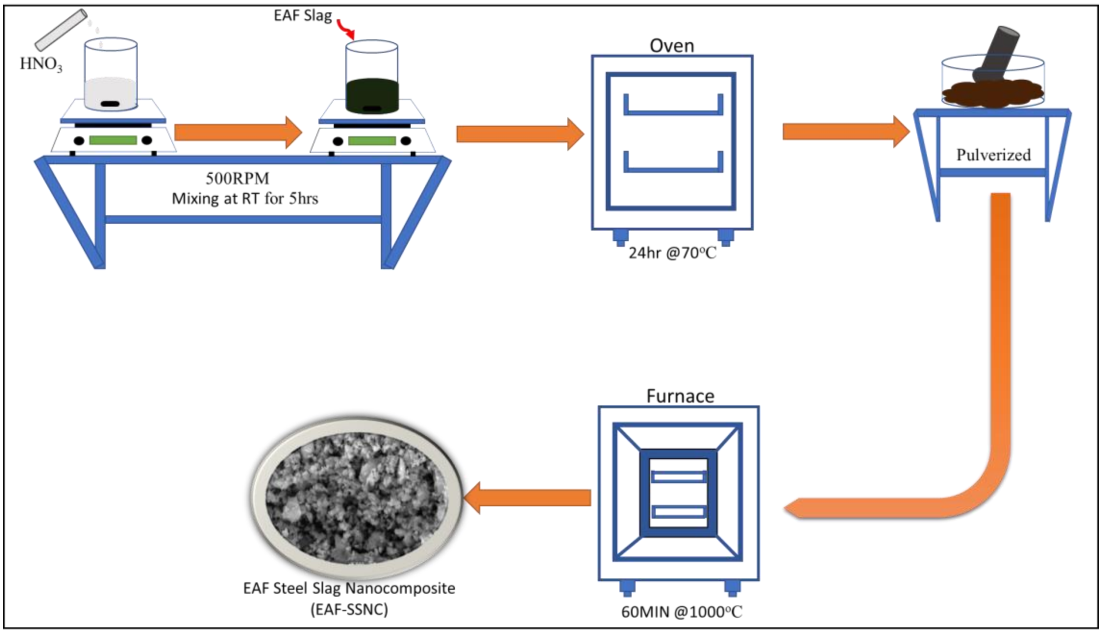

**Fig. 1: Schematic diagram of the preparation EAF-SSNC catalyst**

### 2.2.2 Characterization Techniques

The composition, including the Chemical and elemental components of the prepared samples were characterized by Energy-Dispersive X-ray Spectroscopy (JEOL, JEM-2100F, Japan). The prepared sample's microstructure, morphology, and nanostructure were analyzed using a scanning electron microscope (JEOL JSM-6010LV SEM, Japan). Transmission electron microscope (TEM) was used to obtain high-resolution images. The bond and the functional groups of samples were also examined using Fourier Transform Infrared Spectrometer (Shimadzu FTIR-8400s, Japan). The crystallographic information of the milled EAF slag and EAF-SSNC were also examined using X-ray diffraction with a 1.54 Å, Cu-Kα radiation beam (Shimadzu XRD-6100, Japan). Furthermore, the total organic carbon (TOC) levels were determined using a TOC analyzer (Shimadzu TOC-L, Japan).

## 3. RESULT AND DISCUSSION

### 3.1 Characterization of the Prepared nanocomposite

### 3.1.1 SEM, TEM and EDX

Fig. 2(a, b, c) shows SEM and EDX images of the steel slag nanocomposite (EAF-SSNC) analyzed using FE-SEM. This was done to examine the surface morphology of the prepared EAF-SSNC catalyst sample. As shown in Fig. 2b, at 5,000 magnifications, the findings indicate that the EAF-SSNC has a spherical and heterogeneous form and structure. Wide macropores and connected grains may also be seen in the SEM image of the 20,000 magnifications as depicted in Fig. 2a

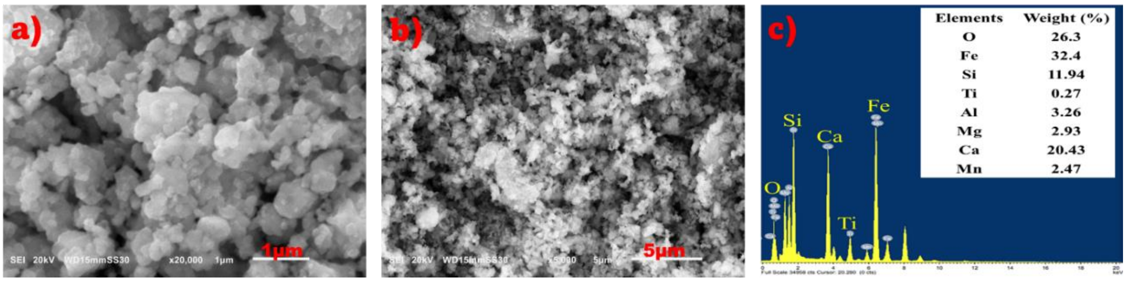

**Fig. 2: SEM and EDX images of SSNC**

The EdX analysis of the SSNC as shown in Fig.2c reveal that SSNC contain around 26.3 wt% of O, 32.4 wt% of Fe, 11.94 wt% of Si, 0.27 wt% of Ti, 3.26 wt% of Al, 2.93 wt% of Mg, 20.43 wt% of Ca and 2.47 wt% of Mn.

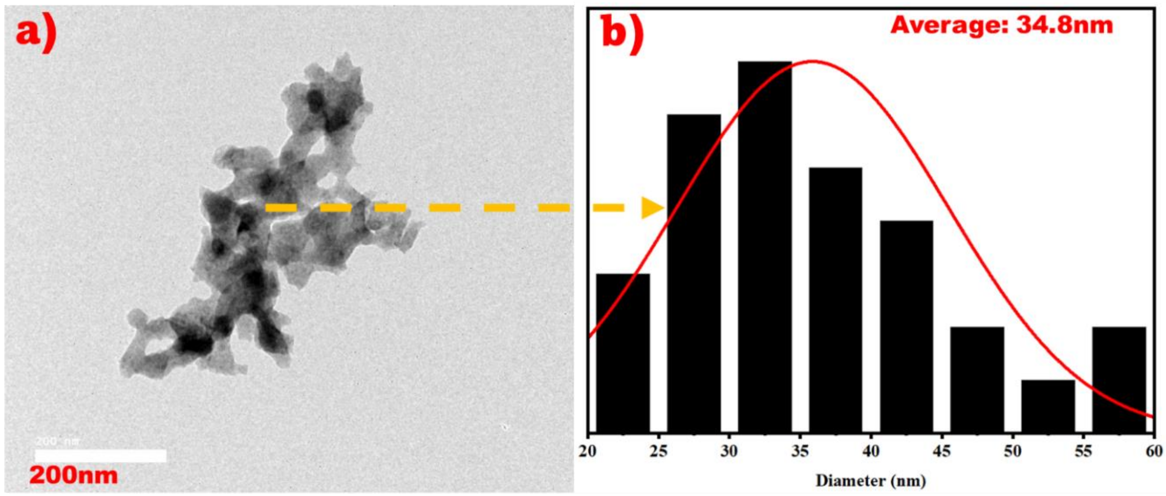

**Fig. 3: (a) TEM images and (b) particle size distribution of EAF-SSNC**

In oder to identify the particle interation and distribution of the nanocomposite, the EAF- SSNC was further use to study the morphology of the prepared samples and the result are depicted in Fig. 3 (a, b). The TEM image of SSNC nanocomposite showns a distinct distribution of the nanocomposite with a avarage particle size of 34.8nm as shown in Fig 3(b) of the particle size distribution curve.

### 3.1.3 FTIR Analysis of the samples

The variations in vibrating peaks for milled EAF-Slag and the prepared EAF-SSNC were tracked using FTIR spectra (spectral ranging from 500-4000cm$^{-1}$). It emerged in the milled EAF-Slag for both the stretching vibration of the O-H peak at 3436 cm$^{-1}$ and the bending vibration of the H-O-H absorption peak at 1638 cm$^{-1}$, as shown in Fig 4 (a). The former and the latter might be associated with chemically bonded water(Bai *et al*., 2018).

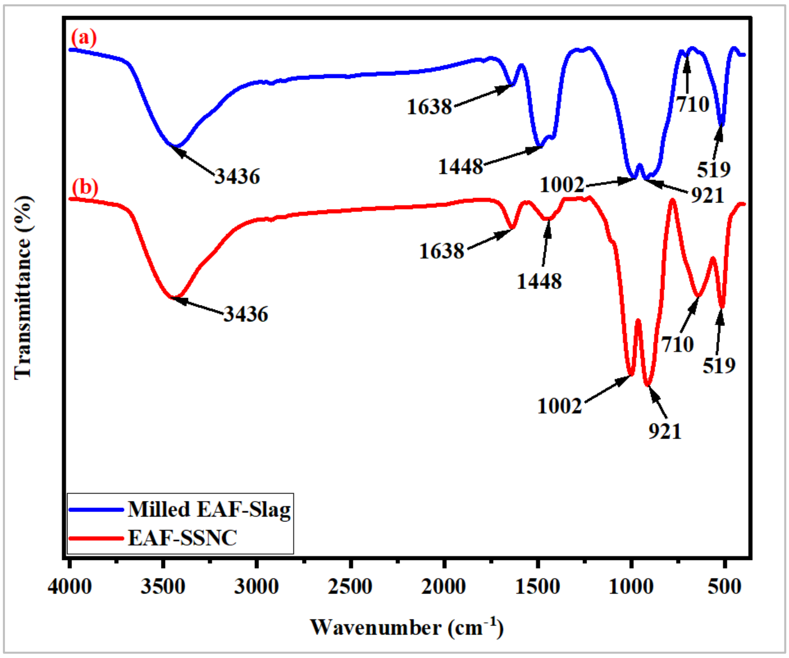

**Fig. 4: FTIR of (a) the EAF milled slag and (b) the EAF-SSNC**

These showed that crystallization and adsorption water were present in the milled EAF-Slag, and the same occurrences were seen in EAF-SSNC, as shown in Fig 4 (b). Furthermore, there was a distinctive absorption peak of about 1487cm$^{-1}$ in Fig 4(a), whose intensity was reduced, and a certain displacement occurred in Fig 4 (b). This might be ascribed to the milled EAF-slag chemical and physical interaction with the $HNO_3$ and the heat treatment. This diminished the milled EAF-slag lattice deformation and vibration, reducing the corresponding stretching vibration C-O modes, which generally arise if a sample increase in CaO content (Jeon *et al*., 2021) (Ma *et al*., 2019). Additionally, the absorptions peak 1002 cm$^{-1}$ and 710cm$^{-1}$ are features of

Si-O and Si-O-Al stretching modes whose vibration stretch increases in Fig 4 (b), indicating an increase in silica and silicate content (Sanad *et al*., 2021) (Bai *et al*., 2018). The bond around 519 cm$^{-1}$ is a vibration of Fe-O, Mg-O, Ti-O, and other metal-oxide (Sarkar *et al*., 2019).

### 3.1.4 XRD Analysis of the samples

The samples' X-ray diffraction patterns were examined using the Hanawalt System for Joint Committee for Powder Diffraction Standards (JCPDS). Fig.5 illustrates the XRD patterns of the milled EAF-slag and the prepared EAF-SSNC. Fig. 5 (a) illustrates the complex composition of milled EAF-slag, which is mostly composed of Andradite (Ca3Fe2O12Si3, PDF No. 00-003-1136), Esseneite (AlCaFeO6Si PDF No. 00-040-0496), Hematite ($Fe_2O_3$, PDF No. 00-024-0072), Larnite (Ca2SiO4, PDF No. 00-006-0476), Laihunite (Fe1.5O4Si, PDF No. 01-078-1435) and Calcite (CaCO3 PDF No.00-003-0569).

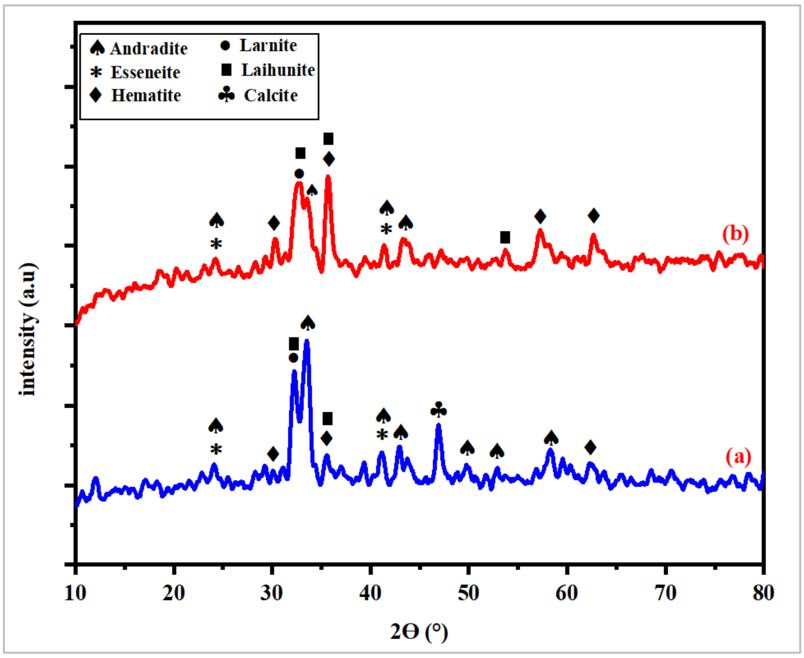

**Fig. 5: XRD patterns of the (a) Milled EAF-slag and the Prepared (b) EAF-SSNC**

Their phase diffraction peaks were strong, with some overlapping peaks of low intensity showing that the EAF slag composition had a considerable number of different crystal structures. Several further studies have observed comparable XRD patterns for EAF slag (Tossavainen *et al*., 2007) (Yildirim and Prezzi, 2011) (Nicolae *et al*., 2007). In Fig. 5 (b), the crystallization diffraction peak centered at 2Θ of 47˚ for the Calcite (CaCO3 PDF No.00-003-0569) vanished with an increase in the Hematite ($Fe_2O_3$, PDF No. 00-024-0072) peak at 35.56˚. Indicating some degree of physical and chemical interaction between the milled EAF-slag and $HNO_3$, as well as a lattice change in crystallinity after heat treatment at 1000˚ C. As a result, the bonding strength of EAF-Slag was increased, which corresponds with the FTIR and EDX result. Additionally, Fig 5(b) included a narrow diffraction peak centered at 2Θ of 30.46˚, 57.14˚ and 62.76˚ showing that the hematite content was increase by a crystalline three-dimensional network structure. These findings suggest that the use of $HNO_3$ has a significant effect on the growth of the hematite phase formed after heat treatment. Owing to the fact that hematite is recognized as a good photocatalyst in visible light and might have a good $CO_2$ reduction due to the presence of hematite as the predominant phase in the prepared EAF-SSNC(Safo *et al*., 2022a) (Ali *et al*., 2020).

### 3.1.5 Optical properties

UV-vis spectroscopy was used to determine the optical absorbance, reflectance, and band gap energy of the prepared EAF-SSNC. The absorbance and reflectance spectra in the range of (200-2000 nm) of EAF-SSNC are shown in Fig.6(a). The characteristic ripples in the spectrum suggest light interference. The considerable decline in reflectance and increase in the absorbance above 742 nm may be attributed to light absorption by the EAF-SSNC nanocomposite followed by electron excitation (Sun *et al*., 2020). The result indicates that the EAF-SSNC produced could absorb light in both the UV and visible regions.

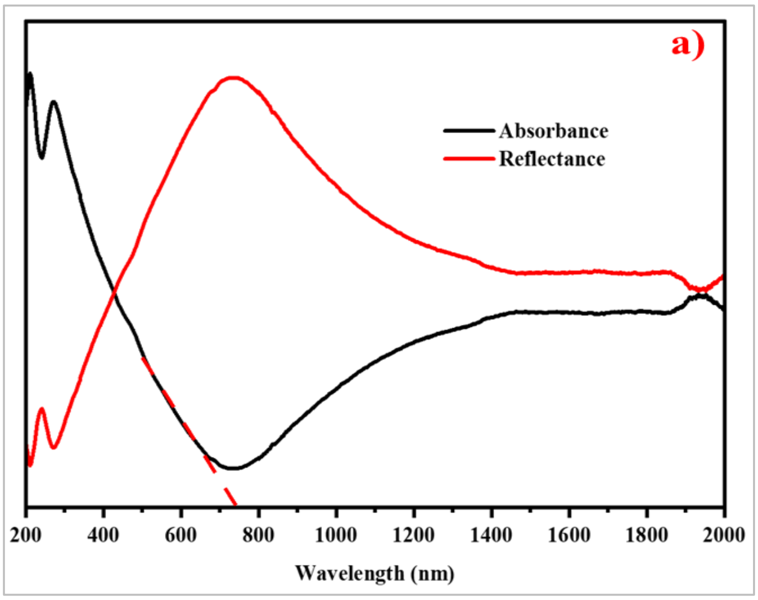

**Fig. 6: UV-Vis DRS spectra of Absorbance and Reflectance**

Moreover, the maximum optical absorption wavelength was 742 nm. The bandgap energy (Eg) of the prepared EAF-SSNC was determined using Eq. (1) (Sunkara and Botsa, 2019).

$$E_g = hc/\lambda = 1240/\lambda \qquad (1)$$

where 'λ' denotes the maximum absorption wavelength. As shown in Fig.6a, the bandgap of the EAF-SSNC nanocomposite is 1.67eV. This might be explained by creating a nanocomposite of various metal oxides from the EAF slag with acid treatment, which produces a predominant amount of $Fe_2O_3$ with a bandgap of 2.2 eV showing a redshift and thus capturing more visible light (Sunkara and Botsa, 2019). This means that the prepared EAF-SSNC might exhibit $CO_2$ reduction under visible light.

### 3.4 Application of the Produce Novel Catalyst for $CO_2$ reduction

The produced catalyst was accessed on its ability to convert $CO_2$ into a useful solar fuel using a continuous flow photochemical reactor.

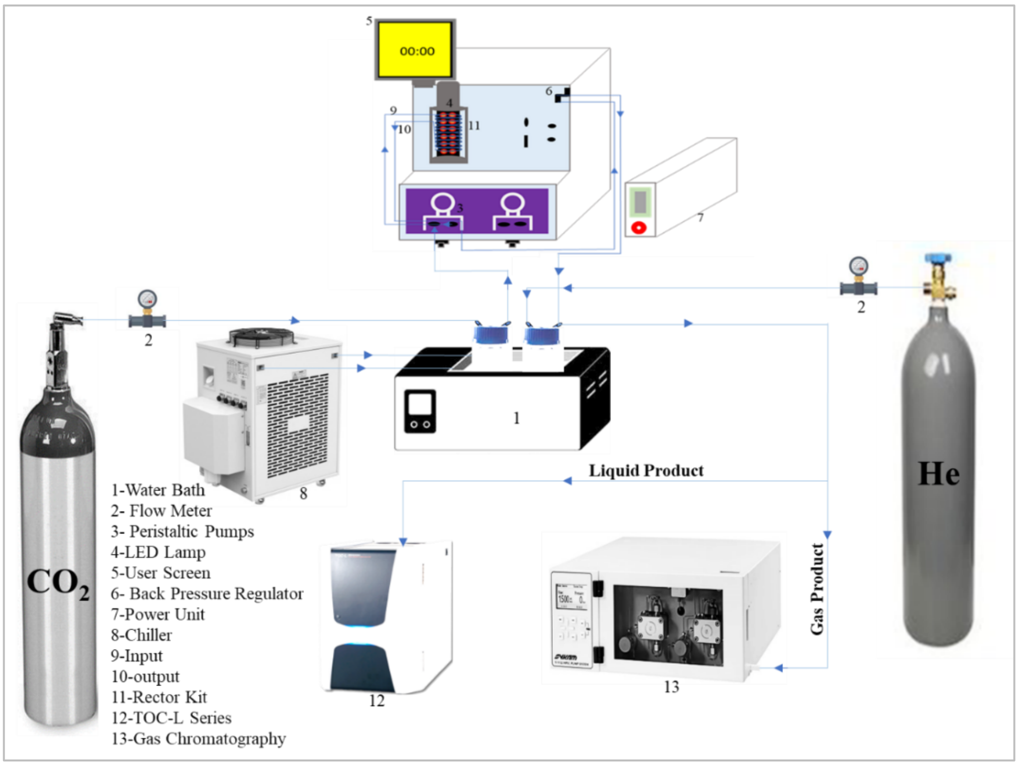

**Fig. 7: Schematic Diagram of the $CO_2$ reduction Experimental Setup**

As shown in Fig. 7, the reduction of $CO_2$ with water was carried out using a UV inner light irradiation system. The fabricated reactor has a 10 ml volume capacity and channels with an inner diameter of 1.3 mm made of fluorinated ethylene propylene (FEP) tubing with thin walls that enable light to pass through.

The source of the photo was a LED lamp with a wavelength of 365 nm. This was done to save energy during the photocatalytic reduction process. The fabricated reactor had several benefits, including the ability to operate in either cooling or heating modes, consistent interior irradiation, and a high volume-to-surface area ratio that enhances mass transmission and photon. The experiment was conducted using ultrasonicated mixed 60mg/L of the EAF-SSNC nanocatalyst and 65ml volume of deionized water. At an average flow rate of 35 ml/min, pure $CO_2$ from the $CO_2$ cylinder was bubbled through the dispersed catalyst for 30 min under a controlled cooled water bath before illumination to increase the solubility of $CO_2$ in the mixture and to guarantee total saturation. The UV LED lamp was switched on when the flow had stabilized, and the pump in the reactor system was used to feed the suspension into the reactor kit at the 500 µl/min flowrate for the photocatalytic reduction and conversion to take place.

After the photocatalytic activity in the rector kit, the products were collected, and the gas product was separated from the liquid product into a gas bag using helium (He) as a gas carrying of flowrate 20ml/min for offline analysis. Analysis was conducted using a gas chromatography analyzer (GC, Shimadzu 2014, Japan) in conjunction with a thermal conductivity detector (TCD) and a micro-packed column Shin Carbon ST (USA Restek, ID 2 mm, length 2m). After the gas bag was examined, no $CH_4$ nor CO was found. Additionally, the gas chromatography analyzer did not detect hydrogen gas ($H_2$), suggesting that its concentration was too low to be detected or used in the reaction process. Furthermore, the cold trap in a water bath was used to confirm that all released organic vapors remained in the liquid phase. The liquid products were qualitatively assessed after extraction and filtration using GC-mass spectroscopy (MS) and quantitatively evaluated using a total organic carbon analyzer (Japan, TOC-L series, Shimadzu) by employing the Nash Technique (Kometani *et al.*, 2017)(Nabil *et al.*, 2022).

The EAF-SSNC photoreduction ability was analyzed at different dosages from 10-60mg/L, 30°C reactor temperature, 500 µl/min flowrate, and 60ml of water volume, as shown in Fig. 8 and 9.

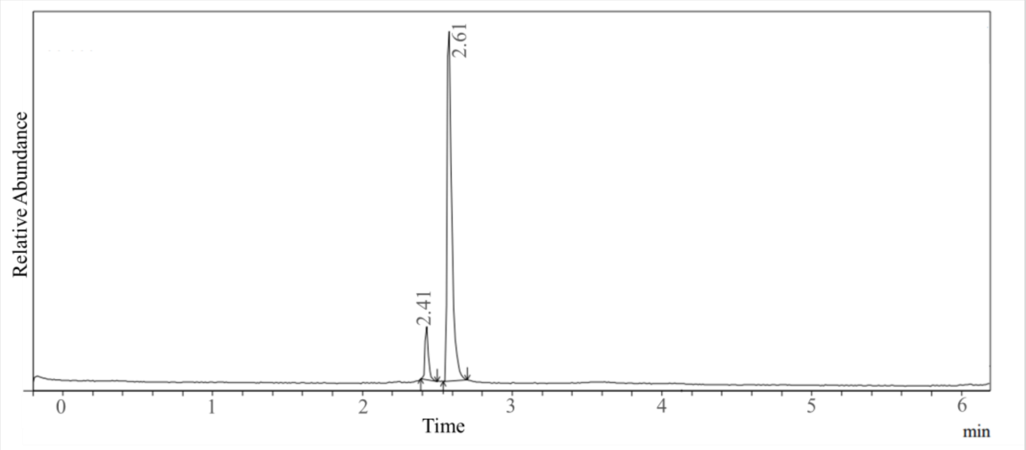

**Fig. 8: The GC/MS chromatographic peaks for methanol at 2.61 minutes and formaldehyde at 2.41 minutes [condition: 30mg/L EAF-SSNC dose, 30°C reactor temperature, 500 µl/min flow rate, and 60ml of water volume]**

The result after the GC/MS analysis indicated that much of the product from the photocatalytic process was methanol with a minor amount of formaldehyde, as shown in Fig.8. Methanol is preferred to gaseous products due to its transportability, storage capacity, and applicable as industrial fuel (Kometani *et al.*, 2017)(Bo *et al.*, 2020). Moreover, the quantitative analysis of the product with a TOC analyzer indicated that increasing the amount of EAF-SSNC dosage increased the amount of TOC, and this resulted in converting more of the $CO_2$ into methanol and formaldehyde, as shown in Fig. 8, but access dosage of the catalyst results in a low amount of TOC. This can be attributed to the fact that an increase in the catalyst dosage above its threshold prevents incident light from researching the catalyst surface to cause an electron to move from the valence band into the conducting band to create an atmosphere for the reduction process of $CO_2$ (Bo *et al.*, 2020)(Safo *et al.*, 2022a).

Nevertheless, the result indicates that EAF-SSNC nanocomposite could convert $CO_2$ into a reusable product due to the chemical composition of the nanocomposite catalyst as elaborated from the EDX, XRD, FTIR, and SEM results.

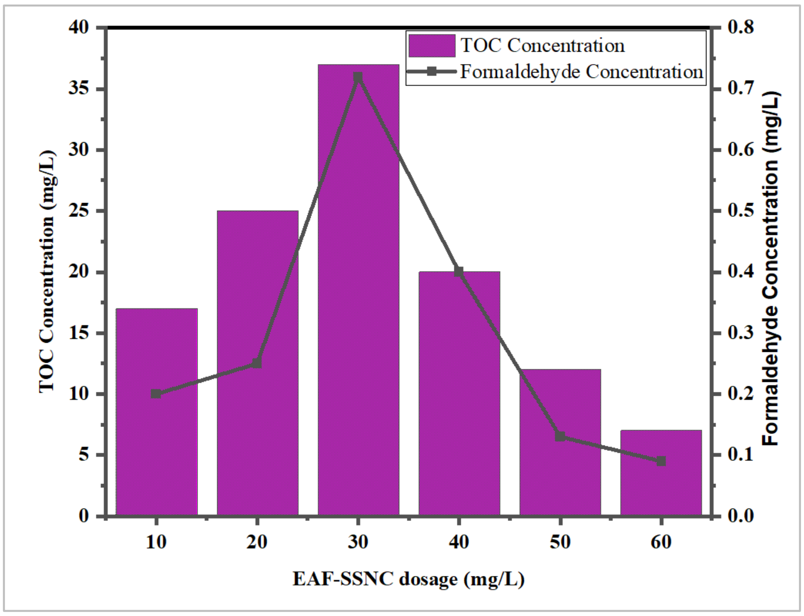

**Fig. 9: A plot of different EAF-SSNC catalyst dosages on TOC and formaldehyde [condition: 30°C reactor temperature, 500 µl/min flow rate, and 60ml of water volume]**

### 3.41 Mechanism of $CO_2$ reduction with EAF-SSNC Catalyst

The $CO_2$ photoreduction mechanism occurs in two phases. Firstly, when an amount of $CO_2$ is absorbed in water, and secondly when $H_2O$ and $CO_2$ are absorbed on the surface of EAF-SSNC. That is, the reduction of $CO_2$ took place at a time when the light was incident on the EAF-SSNC catalyst surface, as depicted in Fig 10. Since the photon of the incident light was greater or equal to the bandgap of the EAF-SSNC catalyst (1.67ev), the electron in the valance band (VB) of the catalyst got excited and moved into the conducting band (CB), creating holes in the VB and free electron in the CD as illustrated in Eqs. (2).

$$\text{EAF-SSNC} + hv \rightarrow h^+_{VB}(\text{EAF-SSNC}) + e^-_{CB}(\text{EAF-SSNC}) \quad (2)$$

The holes in the VB reacted with water molecules under the oxidation and consumption process to produce hydroxyl radicals and hydrogen ions, as illustrated in Eqs. (3).

$$H_2O + h^+ \rightarrow H^+ + OH\bullet \quad (3)$$

The produced radicles further reacted with holes to produce oxygen, as illustrated in Eqs. (4).

$$H_2O + OH\bullet + 3h^+ \rightarrow 3H^+ + O_2 \quad (4)$$

Furthermore, the produced free electron in the conducting band reacted with dissolved $CO_2$ on the surface and in the water under the reduction process to produce methanol and other environmentally friendly hydrocarbons such as formaldehyde, as illustrated in Eqs. (5) and Eqs. (6)

$$4e^- + CO_2 + 4H^+ \rightarrow H_2O + HCHO \quad (5)$$

$$6e^- + CO_2 + 6H^+ \rightarrow H_2O + CH_3OH \quad (6)$$

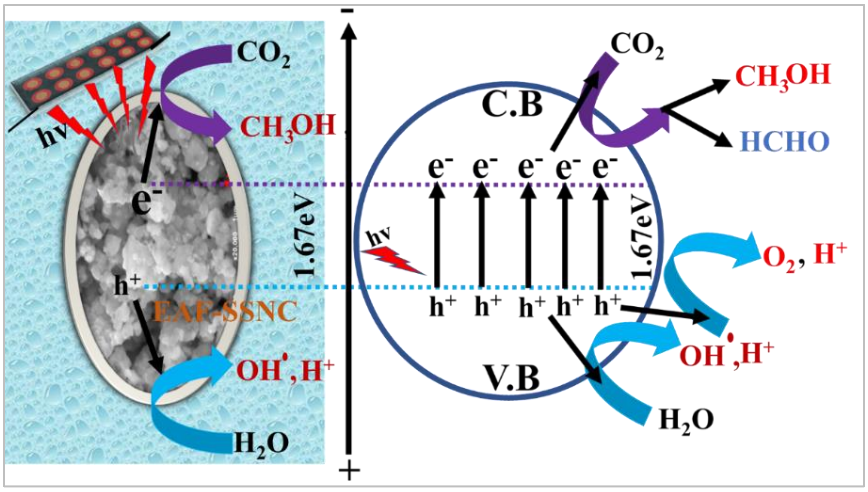

**Fig. 10: Mechanism of $CO_2$ reduction using EAF-SSNC photocatalyst**

This was possible because the EAF-SSNC is made up of different photocatalysts such as $Fe_2O_3$, $SiO_2$, and $TiO_2$ combined with other metal oxides, which was produced using a solvothermal preparation technique into a nanocomposite semiconductor with a band gap of 1.67eV as depicted from the XRF and bandgap analysis (Safo *et al*., 2022a). This enhanced the nanocomposite's ability to absorb enough photos greater than its band gap to initiate the electron-hole per process resulting in the reduction of $CO_2$ into a useful product.

## 5.0 Contribution of the study towards the achievement of SDGs

This study has solved two major environmental problems in many countries, as illustrated in Fig 11. The first is reducing the large amount of slag waste which has caused environmental issues for many years. Secondly, it has converted $CO_2$ into a useful product. Furthermore, regarding the sustainable development goals (SDGs), reducing and converting $CO_2$ into methanol and formaldehyde, which are also low-cost fuels, will help solve global warming problems which result in climate change. This will help ensure 'Climate Action (SDG 13)', 'Affordable and Clean Energy (SDG 7)', and 'Decent work and Economic growth (SDG 8)'.

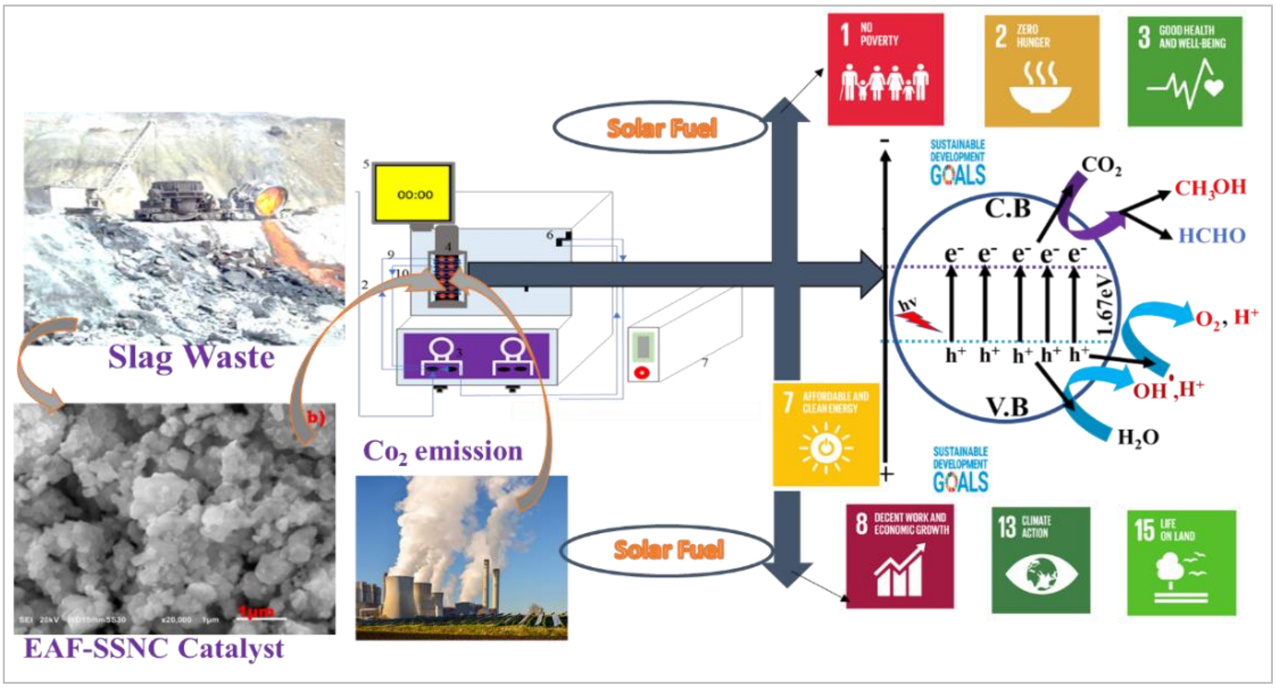

**Fig. 11: Solving environmental problems while meeting the Sustainable development goals (SDG)**

Moreover, water resources will not dry up, and this will ensure irrigation activity in the agriculture sector, producing more food and increasing farmers' income, hence achieving 'No poverty (SDG 1)' and 'No Hunger (SDG 2)'. In addition, the produced nanocomposite catalyst from the steel waste will achieve ‘Good health and wellbeing (SDG 3)"and 'Life on land (SDG 15)'.

## 6.0 CONCLUSION

Industrial slag waste was synthesized into an EAF-SSNC catalyst and utilized for $CO_2$ reduction. Characterization of EAF-SSNC, which include Energy-Dispersive X-ray Spectroscopy (EDX), X-ray diffraction (XRD), Fourier Transform Infrared Spectrometer (FTIR), scanning electron microscope (SEM), and UV-vis spectrophotometer was achieved. The result demonstrated that the catalyst was stable and functioned as a nanocomposite photocatalyst with a band gap of 1.67Ev.

Moreover, EAF-SSNC achieved 37mg/L TOC concentration in the $CO_2$ reduction with high peak production of methanol, a solar fuel applicable in many industries. Finally, the implications of utilizing steel slag for $CO_2$ reduction extend beyond environmental benefits. By repurposing industrial waste, this research contributes to the circular economy and aligns with sustainable development goals, particularly in addressing poverty and hunger (SDG 1 and SDG 2) through improved agricultural irrigation and productivity. Furthermore, the development of this nanocomposite supports good health and well-being (SDG 3) by potentially mitigating climate change effects and promotes life on land (SDG 15) by reducing pollution associated with steel slag disposal.

**Acknowledgments**

The authors thank the support of all collaborated institutions for the success of this project.

**Disclaimer:** None

**Competing Interests:** None

**Source of Funding:** None

## REFERENCES

- Ali, A.S., Khan, I., Zhang, B., Nomura, K., Homonnay, Z., Kuzmann, E., Scrimshire, A., Bingham, P.A., Krehula, S., Musić, S., Akiyama, K., Kubuki, S., 2020. Photo-Fenton degradation of methylene blue using hematite-enriched slag under visible light. J. Radioanal. Nucl. Chem. 325, 537–549. https://doi.org/10.1007/s10967-020-07238-x
- Bai, T., Song, Z.G., Wu, Y.G., Hu, X. Di, Bai, H., 2018. Influence of steel slag on the mechanical properties and curing time of metakaolin geopolymer. Ceram. Int. 44, 15706–15713. https://doi.org/10.1016/j.ceramint.2018.05.243
- Bo, Y., Gao, C., Xiong, Y., 2020. Recent advances in engineering active sites for photocatalytic CO2 reduction. Nanoscale 12, 12196–12209. https://doi.org/10.1039/d0nr02596h
- Chen, J., Xing, Y., Wang, Y., Zhang, W., Guo, Z., Su, W., 2022. Science of the Total Environment Application of iron and steel slags in mitigating greenhouse gas emissions : A review. Sci. Total Environ. 844, 157041. https://doi.org/10.1016/j.scitotenv.2022.157041
- Dananjayan, T., Andimuthu, R., Kandasamy, R., 2022. Utilization of steelmaking slag for carbon capture and storage with flue gas. Environ. Sci. Pollut. Res. 51065–51082. https://doi.org/10.1007/s11356-021-17493-4
- Das, B., Prakash, S., Reddy, P.S.R., Misra, V.N., 2007. An overview of utilization of slag and sludge from steel industries. Resour. Conserv. Recycl. 50, 40–57. https://doi.org/10.1016/j.resconrec.2006.05.008
- Fusco, C., Casiello, M., Pisani, P., Monopoli, A., Fanelli, F., Oberhauser, W., Attrotto, R., Nacci, A., Accolti, L.D., 2022. Steel slag as low - cost catalyst for artificial photosynthesis to convert - CO 2 and water into hydrogen and methanol. Sci. Rep. 1–11. https://doi.org/10.1038/s41598-022-15554-3
- Jeon, I.K., Kim, H.G., Jakhrani, S.H., Ryou, J.S., 2021. Evaluation of the microstructure, mechanical, and durability properties of alkali-activated slag-based mortar with light-burnt dolomite powder. J. Mater. Res. Technol. 13, 2220–2228. https://doi.org/10.1016/j.jmrt.2021.06.024
- Kang, L., Zhang, Y.J., Wang, L.L., Zhang, L., Zhang, K., Liu, L.C., 2015. Alkali-activated steel slag-based mesoporous material as a new photocatalyst for degradation of dye fromwastewater. Integr. Ferroelectr. 162, 8–17. https://doi.org/10.1080/10584587.2015.1037197
- Kometani, N., Hirata, S., Chikada, M., 2017. Photocatalytic reduction of CO2 by Pt-loaded TiO2 in the mixture of sub- and supercritical water and CO2. J. Supercrit. Fluids 120, 443–447. https://doi.org/10.1016/j.supflu.2016.05.031
- Li, Z., Xing, Y., Ma, M., Su, W., Cui, Y., Tian, J., Fei, F., 2024. Towards the co-benefits of carbon capture , utilization and sequestration : A life cycle assessment study for steel slag disposal. J. Clean. Prod. 443, 141166. https://doi.org/10.1016/j.jclepro.2024.141166
- Ma, H., Zhu, H., Yi, C., Fan, J., Chen, H., Xu, X., Wang, T., 2019. Preparation and reaction mechanism characterization of alkali-activated coal gangue-slag materials. Materials (Basel). 12. https://doi.org/10.3390/ma12142250
- Manchisi, J., Matinde, E., Rowson, N.A., Simmons, M.J.H., Simate, G.S., Ndlovu, S., Mwewa, B., 2020. Ironmaking and Steelmaking Slags As Sustainable Adsorbents For Industrial Effluents And Wastewater Treatment: A critical review of properties, performance, challenges and opportunities. Sustain. 12, 1–47. https://doi.org/10.3390/su12052118
- Moon, E., Cheol, Y., 2018. Development of carbon-capture binder using stainless steel argon oxygen decarburization slag activated by carbonation. J. Clean. Prod. 180, 642–654. https://doi.org/10.1016/j.jclepro.2018.01.189
- Nabil, S., Shalaby, E.A., Elkady, M.F., Matsushita, Y., El-Shazly, A.H., 2022. Optimizing the Performance of the Meso-Scale Continuous-Flow Photoreactor for Efficient Photocatalytic CO2 Reduction with Water Over Pt/TiO2/RGO Composites. Catal. Letters. https://doi.org/10.1007/s10562-021-03915-y
- Narindri, B., Winayu, R., Hsieh, H., Chu, H., 2024. Capacity of Ca-based slags for carbon capture. J. Clean. Prod. 460, 142542. https://doi.org/10.1016/j.jclepro.2024.142542
- Nicolae, M., Vîlciu, I., Zăman, F., 2007. X-ray diffraction analysis of steel slag and blast furnace slag viewing their use for road construction. UPB Sci. Bull. Ser. B Chem. Mater. Sci. 69, 99–108.
- Safo, K., Badry, H.N., 2024. Novel Photocatalytic Reduction of CO 2 into Solar Fuel Under a Continuous Flow Photoreactor Using Nano-Engineered Slag Catalyst †.
- Safo, K., Noby, H., Matatoshi, M., Naragino, H., 2022a. Statistical optimization modeling of organic dye photodegradation process using slag nanocomposite. Res. Chem. Intermed. https://doi.org/10.1007/s11164-022-04807-5
- Safo, K., Noby, H., Matatoshi, M., Naragino, H., El-Shazly, A.H., 2022b. Solvothermal Prepared Slag Nanocomposite as a Catalyst for Organic Dye Photodegradation. Key Eng. Mater. 931, 125–130. https://doi.org/10.4028/p-u25360
- Safo, K., Noby, H., Mitsuhara, M., Naragino, H., 2023a. Novel solar simulated photocatalytic heterolysis of pharmaceutical wastewater via slag

nanocomposite immobilization : Optimization using response surface methodology. Water Pract. Technol. 18, 2315–2328. https://doi.org/10.2166/wpt.2023.152

- Safo, K., Noby, H., Mitsuhara, M., Naragino, H., El-Shazly, A.H., 2023b. H2O2 assisted steel slag nanocomposite for degradation of organic pollutant in an advanced oxidation process for suspension and Spin-Coated mode. Environ. Nanotechnology, Monit. Manag. 20, 100836. https://doi.org/10.1016/j.enmm.2023.100836
- Safo, K., Rubangakene, N.O., Noby, H., El-Shazly, A.H., 2025. Photocatalytic purification of dye-containing wastewater using a novel embedded hybrid TiO2–slag catalyst heterojunction nanocomposite coupled with statistical models: A sustainable and techno-economic approach. Water Sci. Eng. https://doi.org/10.1016/j.wse.2025.02.003
- Sanad, M.M.S., Farahat, M.M., El-Hout, S.I., El-Sheikh, S.M., 2021. Preparation and characterization of magnetic photocatalyst from the banded iron formation for effective photodegradation of methylene blue under UV and visible illumination. J. Environ. Chem. Eng. 9, 105127. https://doi.org/10.1016/j.jece.2021.105127
- Saratu, J., Pullin, H., Renforth, P., 2021. Assessing the carbon capture capacity of South Wales ' legacy iron and steel slag. Miner. Eng. 173, 107232. https://doi.org/10.1016/j.mineng.2021.107232
- Sarkar, C., Basu, J.K., Samanta, A.N., 2019. Synthesis of MIL-53(Fe)/SiO2 composite from LD slag as a novel photo-catalyst for methylene blue degradation. Chem. Eng. J. 377, 0–1. https://doi.org/10.1016/j.cej.2018.08.007
- Sun, Z., Pichugin, V.F., Evdokimov, K.E., Konishchev, M.E., Syrtanov, M.S., Kudiiarov, V.N., Li, K., Tverdokhlebov, S.I., 2020. Effect of nitrogen-doping and post annealing on wettability and band gap energy of TiO2 thin film. Appl. Surf. Sci. 500. https://doi.org/10.1016/j.apsusc.2019.144048
- Sunkara, J.R., Botsa, S.M., 2019. SnO2/Fe2O3/Ag Nanocomposite via Hydrothermal Approach: A Novel Highly Efficient Photodegradation of Eosin Yellow and Brilliant Green Dyes Under Visible Light Irradiation. Chem. Africa 2, 635–644. https://doi.org/10.1007/s42250-019-00086-7
- Tossavainen, M., Engstrom, F., Yang, Q., Menad, N., Lidstrom Larsson, M., Bjorkman, B., 2007. Characteristics of steel slag under different cooling conditions. Waste Manag. 27, 1335–1344. https://doi.org/10.1016/j.wasman.2006.08.002
- Tsakiridis, P.E., Papadimitriou, G.D., Tsivilis, S., Koroneos, C., 2008. Utilization of steel slag for Portland cement clinker production. J. Hazard. Mater. 152, 805–811. https://doi.org/10.1016/j.jhazmat.2007.07.093
- Yildirim, I.Z., Prezzi, M., 2011. Chemical, mineralogical, and morphological properties of steel slag. Adv. Civ. Eng. 2011. https://doi.org/10.1155/2011/463638
- Yu, J., Wang, K., 2011. Study on Characteristics of Steel Slag for CO 2 Capture 5483–5492.
- Zhang, Y., Yu, L., Cui, K., Wang, H., Fu, T., 2023. Carbon capture and storage technology by steel-making slags : Recent progress and future challenges. Chem. Eng. J. 455, 140552. https://doi.org/10.1016/j.cej.2022.140552
- Zhao, Q., Liu, C., Mei, X., Saxén, H., Zevenhoven, R., 2025. Research progress of steel slag-based carbon sequestration. Fundam. Res. 5, 282–287. https://doi.org/10.1016/j.fmre.2022.09.023.